

Carbon Dioxide Gasification of Kraft Black Liquor Char in a Laboratory Char Bed Reactor

T. Sean Connolly, A. Co, E. Schwiderke and A. R. P. van Heiningen,

Department of Chemical & Biological Engineering, University of Maine

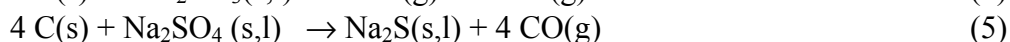
Abstract

In the current study a series of pyrolysis and CO₂ gasification experiments were conducted on a bed of kraft black char under a perpendicular impinging jet. The experiments demonstrated that the char bed carbon gasification rates are externally mass transfer limited. The mass transfer is further decreased by a net molar out-flow caused by the conversion of one mole of reactant CO₂ to two moles of product CO via gasification. Predictions of the mass transfer coefficient using the COMSOL MultiPhysics finite element program were comparable with those obtained from the experimental data.

Introduction

The char bed is perhaps the least understood portion of a kraft black liquor recovery boiler. The comprehensive studies of A.D. Little reported by Merriam & Richardson in 1978 and 1979 still provide most of the present day understanding about the char bed. A one-dimensional model of the mass and energy flows inside the char bed was also developed. The predictions of the model were in general agreement with the experimental results and earlier bed and gas temperature measurements reported by Borg et al. (1974). Data collected suggests that CO₂ gasification plays a key role in consumption of organic carbon in the active layer of the char bed but no comprehensive rate expression was developed.

The char bed combustion processes have been reviewed by Grace and Frederick (1997) and Grace (2001). Based on the experimental studies referred to above, there is a general consensus that the burning rate of the char bed is limited by mass transfer of oxygen and gasification gases (CO₂ and H₂O) and by radiation heat transfer to the bed surface needed for the endothermic carbon consuming reactions (sulfate reduction, gasification and sodium carbonate reduction). These reactions are:



The formation of CO₂ is not included in the overall reactions (4) and (5) because reaction (2) quickly leads to CO formation at the temperatures in the bed. It was realized by Merriam & Richardson (1978) that there is a net outflow of gas from the bed due to formation of two moles of CO per mole of CO₂ consumed in reaction (2). As a result nitrogen would be swept out of bed, and its concentration would be lower than that in a combustion gas. Merriam & Richardson (1978) assumed in their model that reaction (2) would be at equilibrium with carbon present in excess. Additional CO produced by sulfate reaction (5) was also considered, but reactions (3)

and (4) were not. Based on a recent study of gaseous samples collected from a char bed (Connolly & Van Heiningen 2004) it was shown that the change in gas composition inside the bed is consistent with a net outflow of gas from the bed.

In earlier laboratory char bed experiments (Brown et al, 1989 & Kochesfahani et al, 1998) air jets parallel to the bed surface (with or without CO₂ and H₂O added) were used to simulate the primary air jets sweeping over the char bed. Since the reactivity of oxygen with organic carbon is very high, all oxygen reacts at the interface rather than penetrate into the char layer as might occur for CO₂ and steam (Sutinen, Karvinen, & Frederick, 2002). A unique aspect of the two experimental char bed studies is the continual replenishment of organic carbon at the char surface by using a moving bed arrangement. Lee and Nichols (1997) studied gasification of black liquor char by feeding CO₂ through a packed bed of the char. They found that the gasification rate was limited by chemical kinetics below 700°C, but that diffusional limitations became important at higher temperature.

In the present study the interaction between carbon gasification by CO₂ and mass transfer processes was investigated for a black liquor char bed at temperatures of 675 -815°C with a gas jet impinging on its top surface. The measured carbon gasification rate is interpreted in terms of external and internal mass transfer resistances, and the influence of net outflow of gasification gas from the char bed is quantified.

Experimental Setup

The impinging jet reactor set-up is depicted in Figure 1. The feed gas flow system includes mass flow controllers and a coiled heat exchanging tube inside the reactor to deliver an accurate flow and composition of gas preheated to the bed temperature. An Agilent 3000 Micro GC equipped with a TCD cell and two separation columns was used to analyze the product gas for permanent gases, N₂, O₂, CO₂, H₂, CH₄ & CO every three minutes. CO and CO₂ gas concentrations were also continually monitored by an online Siemens CO/CO₂ analyzer. The aluminum oxide cup under the impinging jet contained the bed of pyrolyzed kraft black liquor char. The reactor element was heated by a pottery kiln. Product gases were cooled by a shell and tube heat exchanger followed by water trap filter prior to gas analysis. The gas temperature just below the nozzle and just above the char bed was measured by thermocouples. The inner diameter of the impingement nozzle is 7 mm, the diameter of the char bed is 105 mm, and the distance from the nozzle to the char bed surface is 149.3 mm.

To better understand the CO₂ gasification behavior of the kraft black liquor char bed, five variables were investigated: bed thickness, impinging jet flow rate, gas diffusivity (helium versus nitrogen as carrier gas for reactant CO₂), bed temperature, and CO₂ concentration in the jet. The experimental reactor was brought up to the desired steady state temperature under an impinging flow (1 L/min) of nitrogen. When the desired temperature was reached, CO₂ was added at a flow rate to obtain the desired gas composition and total flow rate. The char bed behavior during the heat up period will be reported as char pyrolysis. The steady state CO₂ gasification conditions are summarized in Table 1.

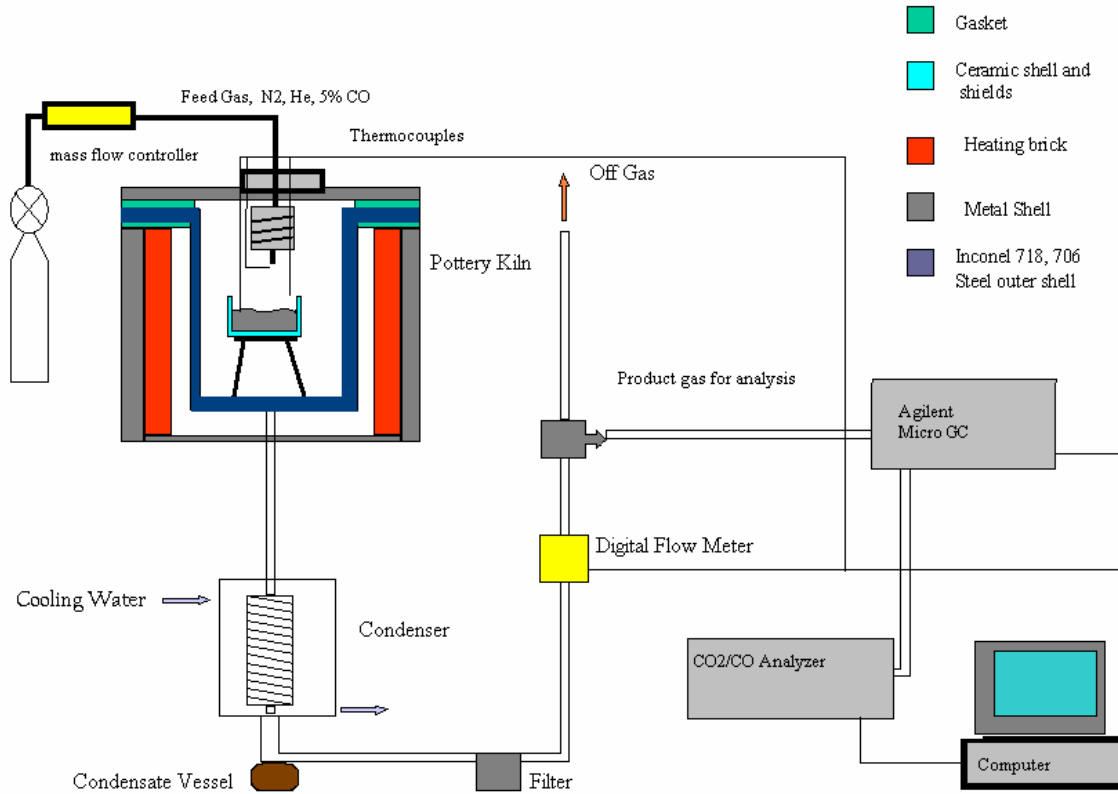


Figure 1. CO₂ Gasification Reactor Setup

Table 1. CO₂ Gasification Experimental Conditions

Experiment	Gasification Gas	Impinging Jet Flow Rate [L/min]	Bed Mass [grams]	Bed Thickness [mm]	Bed Temperature [°C]
1	N ₂ , 10% CO ₂	3.3	100	19	815
2	N ₂ , 44% CO ₂	3.3	100	19	815
3	N ₂ , 89% CO ₂	3.5	100	19	815
4	N ₂ , 83% CO ₂	2.9	50	10	815
5	N ₂ , 84% CO ₂	2.9	200	38	815
6	N ₂ , 15% CO ₂	4.5	100	19	815
7	He, 18% CO ₂	4.1	100	19	815
8	N ₂ , 85% CO ₂	2.9	100	19	675
9	N ₂ , 88% CO ₂	2.8	100	19	750
10	N ₂ , 85% CO ₂	1.0	50	10	815
11	N ₂ , 85% CO ₂	6.0	100	19	815

Data Analysis

The solid residues remaining after gasification were dissolved in water. The dry weight of the solids remaining after dissolution was determined. The following analyses were performed on the solution: cyanate (OCN^-), sulfite (SO_3^{2-}), thiosulfate ($\text{S}_2\text{O}_3^{2-}$) and chloride (Cl^-) using ion chromatography, carbonate (CO_3^{2-}) as CO_2 using headspace gas chromatographic analysis, sodium and potassium using ICP, and hydroxide, sulfide and carbonate using ABC titration. The focus of this paper, however, is on the gas phase results.

Reaction of gasification gas with the reactor wall

Close examination of the effluent gas composition showed that the gasification gases produced by the char bed reacted with the outer reactor vessel made from Inconel. This made it impossible to determine the organic carbon consumption from the CO production rate using the CO_2 gasification reaction (equation 2). A series of experiments were performed with different CO_2 and CO concentrations fed to the empty reactor (Table 2). It was found that excess CO was converted into CO_2 on a one to one molar basis and vice versa.

Table 2. Empty Reactor Experiments with CO and CO_2 Feed

Total Volumetric Feed rate [liters/min]	CO Feed rate [mmole/min]	CO_2 Feed rate [mmole/min]	CO Conversion Rate [mmole/min]	CO_2 Conversion Rate [mmole/min]	Molar ratio CO/CO_2
1.395	8.18	12.39	-1.74	1.71	-0.98
1.498	12.27	12.31	-2.18	2.43	-1.12
1.167	4.09	11.94	-0.22	0.22	-1.02
3.617	10.22	24.50	-4.96	4.59	-0.93
4.005	28.63	118.16	-5.88	7.08	-1.20
3.464	6.13	24.29	-2.01	2.38	-1.18
3.568	10.22	24.29	-3.27	3.27	-1.00
3.799	0	31.08	1.17	-1.24	-1.07

Based on literature information (Da Silva, 1960) it seems likely CO reacted with magnetite (Fe_3O_4) of the Inconel producing CO_2 production by the equilibrium reaction (6):



At 815°C the equilibrium of reaction (6) is shifted towards the right, i.e. it favors CO_2 formation from CO (Table 3). Furthermore this reaction is thermodynamically unfavorable below 375°C , which confirms our finding that 5% CO in the feed to the reactor was stable below 375°C (see Figure 2). This figure also shows that CO in the feed is converted into CO_2 on a one to one molar basis during the heat up of the reactor from about 350 to 600°C . Above 600°C both CO and CO_2 formation occurs due to further pyrolysis and gasification of the black liquor char.

Table 3. Equilibrium Constants for Reduction of Magnetite (Fe_3O_4) by CO (equation 6)

Temperature ($^\circ\text{C}$)	300	400	500	600	700	800	900
Equilibrium Constant (k_{eq})	0.576	1.108	1.684	2.181	2.525	2.692	2.697

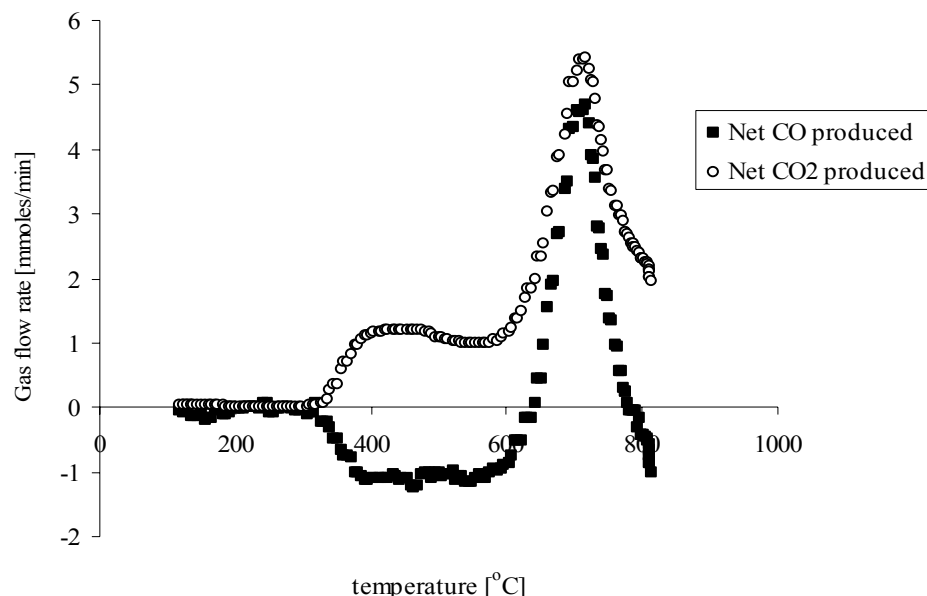


Figure 2. Conversion of CO to CO₂ in Empty Reactor during Heat-Up of 5% CO in N₂

Therefore the organic carbon loss both during heat up (i.e. during pyrolysis) and by gasification can only be quantified by the net gain of carbon in the gas phase since all carbon remains in the gas phase when reaction 6 occurs. Thus the carbon gasification rate may be calculated as:

$$\text{Carbon Release Rate} = \text{Carbon Removal Rate as CO \& CO}_2 - \text{Carbon Feed Rate as CO}_2 \quad (7)$$

An example of this calculation procedure during gasification of the char by CO₂ at 815°C is seen in Figure 3. Also included in Figure 3 is the carbon consumption rate calculated from the CO production rate using equation (2). When comparing the organic carbon consumption rates calculated based on the two methods, one can see that initially the gasification rate calculated from the CO production (equation 2) is smaller than the actual gasification rate calculated by equation (7). The explanation is that CO released from the bed is converted to CO₂ by the reactor wall. When the char bed gasification is nearly completed at about 175 minutes the wall converts Figure 3 also shows that the carbon gasification rate calculated using equation (7) shows more scatter than when calculated from the CO production using equation (2). The explanation is that two large and nearly equal numbers are subtracted from each other when using equation (7). However the overall accuracy of the use of equation (7) for data analysis can be demonstrated by a carbon mass balance. For example, integrating the area under the curve in Figure 4 yields a carbon consumption of 22.76 grams. During heat-up an additional amount of 0.78 grams of organic carbon consumption is released. This adds up to a total of 23.54 grams compared to an initial amount of 24.14 grams at the start of the experiments present in the black liquor char. The difference of 0.60 grams of unreacted carbon remaining in the char at the end of the experiment compares well with the mass of 0.63 grams of insolubles remaining after dissolution of the final char bed in water. This result is shown as experiment 2 in Table 4. The carbon mass balance for the all experiments listed in Table 4 show a good agreement between the calculated weight of unreacted organic carbon at the end of gasification and the weight of insolubles in the final char. This further confirms the validity of the present calculation procedure for the gasification rate.

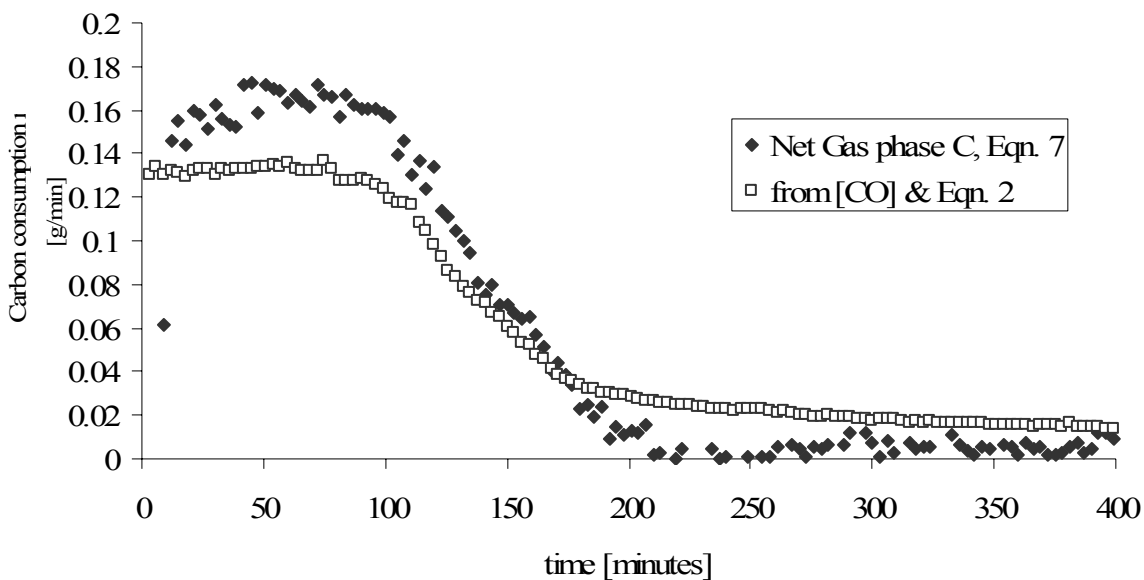


Figure 3. Organic Carbon Consumption Rate Calculated from CO Production (Equation 2) and Net Carbon Release (Equation 7). 44% CO₂ , Total Flow 3.3 L/min, 815°C (Exp. 2)

Table 4 Organic Carbon Mass Balance during Gasification

Exp *	Gasification Time [minutes]	Initial Org Carbon [grams]	Gasified Org Carbon [grams]	Pyrolized Org Carbon [grams]	Org Carbon Calc [grams]	Insoluble Org C [grams]
1	700	26.15	24.50	0.47	1.18	1.12
2	250	24.14	22.76	0.78	0.60	0.63
3	75	25.94	24.83	0.51	0.60	0.49
4	70	12.74	12.01	0.59	0.14	0.16
5	300	48.89	45.86	1.56	1.47	1.44
6	300	24.79	23.23	1.10	0.46	0.92
7	250	24.83	23.58	0.25	1.00	0.79
8	350	24.77	24.33	0.10	0.34	0.70
9	225	25.17	23.46	1.51	0.20	0.64
10	90	12.42	10.43	1.70	0.29	0.49
11	75	25.43	24.25	0.99	0.20	0.39

* For experimental conditions, see Table 1

Theoretical Analysis of Carbon Consumption Rate

Because the experimentally obtained organic carbon consumption rates are small compared to pure chemical kinetics reported in literature (Li & van Heiningen 1990), it is likely that the rates are limited by mass transfer resistances outside and inside the char bed. Therefore it is

appropriate to analyze the data using the shrinking core model (Levenspiel, 1996). In the standard shrinking core model the effect of excess gas generated by the gas-solid reaction is not included. Since flow has a significant effect on the internal and external mass transfer resistance, the derivation of the shrinking core model with the inclusion of this effect is given below.

The molar balance for carbon dioxide when external mass transfer is the rate limiting step is given by equation (8). The left-hand side represents the consumption of CO₂ at the reacting char bed surface. The first term on the right-hand side represents the diffusion transport of CO₂ through the external film of total thickness, δ , while the second term denotes the convective transport of CO₂ due to outflow of excess gasification gas since for every mole of CO₂ consumed, two moles of CO are generated.

$$\frac{1}{S_A} * \frac{dN_{CO_2}}{dt} = D_{CO_2} * \frac{dC_{CO_2}}{dl} - \frac{\phi_V}{S_A} * C_{CO_2} \quad (8)$$

where S_A is the exposed cross-sectional surface area of the char bed (m²); $\frac{dN_{CO_2}}{dt}$ is the CO₂ consumption rate by the char (mol/s); D_{CO_2} is the diffusivity of CO₂ (m²/s) in the gas; $\frac{dC_{CO_2}}{dl}$ is the concentration gradient of CO₂ at the char bed surface of the external gas film, and ϕ_V is the outflow rate of gasification gas (m³/s). ϕ_V is related to the CO₂ consumption rate since two moles CO are produced per mole of CO₂ consumed, or

$$\phi_V = \frac{dN_{CO_2}}{dt} * \frac{R * T}{P} \quad (9)$$

where T and P are the temperature and pressure of the reacting system, and R is the gas constant. Insertion of (8) in (9) gives equation (10).

$$\frac{dN_{CO_2}}{dt} * \frac{1}{S_A} = \frac{D_{CO_2}}{\left(1 + \frac{R * T}{P} C_{CO_2}\right)} * \frac{dC_{CO_2}}{dl} \quad (10)$$

By assuming pseudo steady state for the gasification rate, equation (10) may be integrated from the surface of the char bed (where $C_{CO_2} = 0$) to the external film thickness δ (where $C_{CO_2} = C_{CO_2,bulk}$). By defining the external mass transfer coefficient k_g as (D_{CO_2} / δ) , and using that the carbon conversion $X = N_C / N_{C,0}$, one obtains for the carbon conversion rate, dX/dt :

$$\frac{dX}{dt} = \frac{S_A * k_g * P}{N_{C,0} * R * T} * \ln\left(1 + \frac{R * T}{P} C_{CO_2,bulk}\right) \quad (11)$$

where $N_{C,0}$ is the initial number of moles of organic carbon in the char layer.

The external mass transfer coefficient, k_g , can be determined from the carbon conversion rate calculated using equation (11).

Experimental Results

Effect of Carrier Gas

Figure 4 shows the effect of type of carrier gas on the organic carbon gasification rate versus organic carbon conversion, X (exps 6 & 7). These two experiments were conducted at slightly different impinging velocities and CO_2 concentrations. It can be seen that the gasification rate is higher in helium compared to that in nitrogen. Experimental error in the determination of the amount of organic carbon remaining is the reason for conversion reaching a value larger than 1.0. The results show that the organic carbon consumption rate is relatively constant over a wide range of conversion, X . This is expected if the gasification rate is limited by external mass transfer of CO_2 from the jet to the char bed surface.

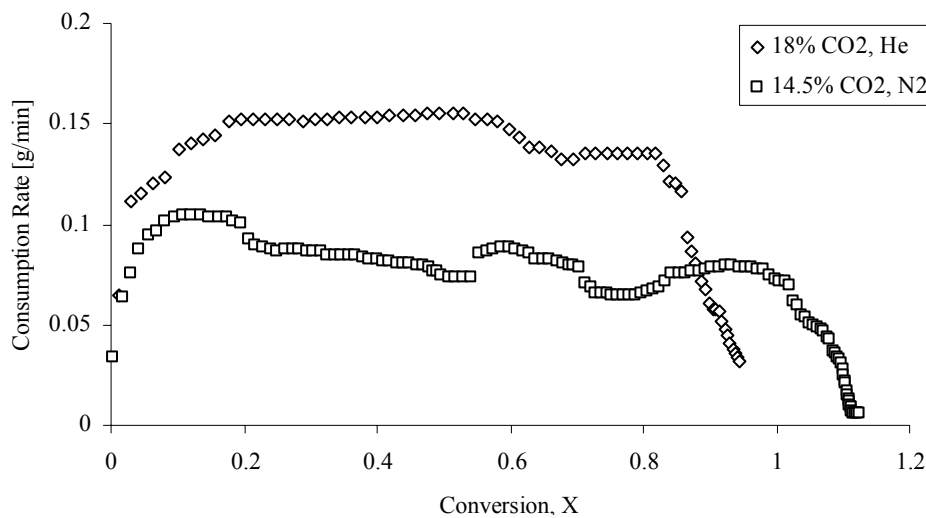


Figure 4 Organic Carbon Consumption Rates at about 15% CO_2 in N_2 or He, $T= 815^\circ\text{C}$

A plot of the conversion X versus time is shown in Figure 5. Values of k_g may be obtained from the slopes of the linear portion of the X - t plots using equation 11 as described earlier.

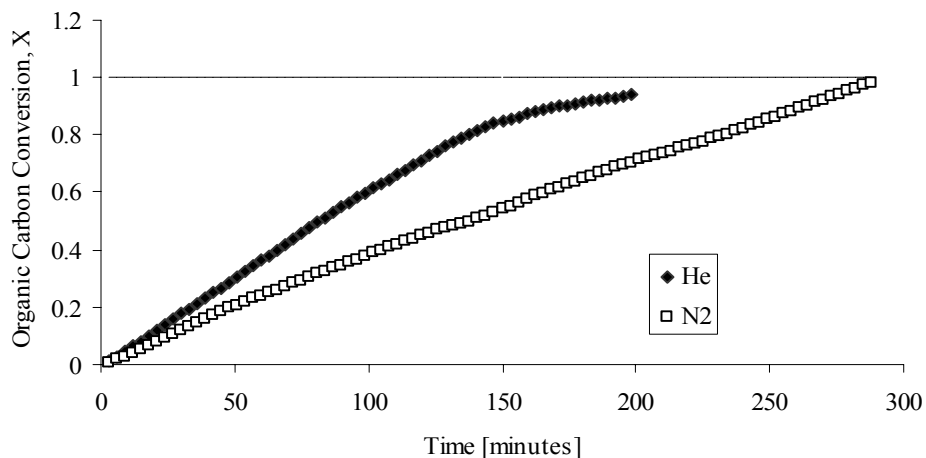


Figure 5 Organic Carbon Conversion at about 15% CO_2 in N_2 or He, $T= 815^\circ\text{C}$

Table 5 summarizes the experimentally determined k_g values for the two experiments. It shows that the value of k_g is higher for gasification in helium.

Table 5 Mass Transfer Coefficients with Different Carrier Gases, T = 815°C

Jet Velocity [L/min]	Carrier	$N_{C,0}$ [moles]	$CO_{2,bulk}$ [mole/m ³]	Slopes of plots [s ⁻¹]	Re	Sc	Experimental k_g [m/s]	$k_{g,0}$ from Eqns 12 – 14 [m/s]
4.1	He	2.05	1.567	1.02×10^{-4}	357	0.24	1.40×10^{-2}	2.04×10^{-1}
4.5	N ₂	1.97	1.148	5.97×10^{-5}	404	0.64	1.10×10^{-2}	1.24×10^{-1}

A significant amount of research exists in the field of heat transfer under jets impinging on flat plates. Heat transfer correlations based on experimental measurements, and numerical solutions of the Navier – Stokes equations have been produced by Popiel et al (1980), and Saad et al (1977) respectively. The heat transfer at the impingement stagnation point, directly below the nozzle at the bed surface expressed as the Nusselt number (Nu_0) is correlated to the Reynolds (Re) and Prandtl (Pr) numbers and the non-dimensional distance between the impinging jet nozzle and impingement surface by equation (12)

$$Nu_0 = (137 - 1.8 * H) * 10^{-3} * Re^{0.75} * Pr^{0.4} \quad (12)$$

where H is the ratio between the nozzle diameter (D_0) and the nozzle tip to impingement surface distance.

The mass transfer coefficient at the stagnation point, $k_{g,0}$, can be calculated from Nu_0 using the analogy between heat and mass transfer for laminar flow of

$$Sh_0 = \left(\frac{Sc}{Pr} \right)^{\frac{1}{3}} * Nu_0 \quad (13)$$

where Sh is the Sherwood number, defined as

$$Sh_0 = \frac{k_{g,0} * D_0}{D_{AB}} \quad (14)$$

The values of $k_{g,0}$ in Table 5 were calculated from equations (12) – (14) using diffusivities, D_{AB} , for CO₂ in nitrogen and helium at 815°C of 1.297×10^{-4} and 4.018×10^{-4} m²/s respectively. It shows the calculated values of $k_{g,0}$ are an order of magnitude larger than the present experimental values of k_g . This is not surprising because k_g is the mass transfer coefficient averaged over the entire impingement surface, and the mass transfer coefficient decreases dramatically going from the stagnation point to the periphery of the bed as will be shown later in this paper. In addition equation (12) does not account for the decreasing effect on the mass transfer coefficient of a net gas flow emerging from the impingement surface due to carbon gasification. However, the calculated values of $k_{g,0}$ are higher in helium than that in nitrogen, just as is found experimentally.

In Figure 4, one can see that the organic carbon consumption rate in the helium experiment decreases rapidly once 80% of the organic carbon is consumed. In the nitrogen experiment the rapid decrease also occurs during the consumption of the last 20%. This behavior may be explained by the non-uniform mass transfer distribution under the impinging jet, with maximum mass transfer at the stagnation point and continuously decreasing values away the stagnation point. This would lead to complete carbon combustion in the stagnation region with still a significant amount of carbon present near the periphery of the bed. In other words, the strong decrease in gasification rate after about 80% organic carbon consumption signifies complete carbon burnout in the stagnation region.

Effect of CO₂ Concentration

Figure 6 shows the effect of CO₂ concentration in the impinging jet on the carbon consumption rate (exps 1, 2 & 3). Increasing CO₂ concentration increases the rate of organic carbon consumption. Each experiment experiences an initial plateau in which external mass transfer resistance is controlling the consumption rate. After approximately 70% of the organic carbon is consumed the final organic carbon burnout is likely controlled by non-uniform organic carbon conversion in the radial direction of the char bed. In order to determine the external mass transfer coefficient, k_g , the organic carbon conversion, X , is plotted versus time in Figure 7 for the three experiments. Table 6 summarizes the experimentally determined k_g values. It shows that the coefficient of external mass transfer, k_g , decreases by about 25% while the CO₂ concentration increases almost nine-fold. This shows that the effect of CO₂ concentration on mass transfer is well described by equation (11). The small decrease in k_g may be the result of a change in the physical properties of the gas in the film layer due to different CO concentrations in the film. For example, the D_{AB} values at 815°C in nitrogen are 1.297×10^{-4} m²/s for CO₂ and 1.679×10^{-4} m²/s for CO. Alternatively the decrease may due to the fact that the gasification rate is higher at higher CO₂ concentration, and thus also the net gas outflow from the char bed. The larger outflow will further decrease the average mass transfer coefficient k_g . The stagnation mass transfer coefficient $k_{g,0}$ determined by equations (12) – (14) is again approximately one order of magnitude higher than k_g for reasons discussed earlier.

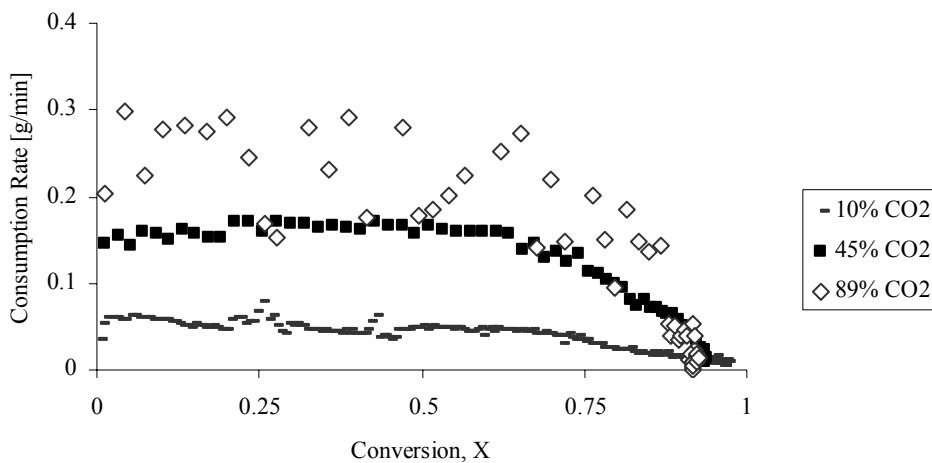


Figure 6. Organic Carbon Consumption Rates, Different CO₂ Concentration, Flow rate 3.3 L/min, T= 815°C

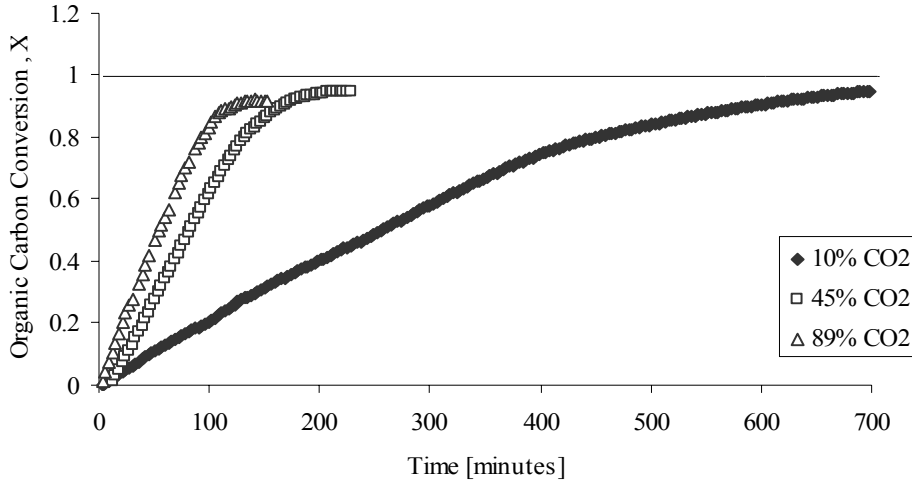


Figure 7. Organic Carbon Conversion, X, Different CO₂ Concentrations, Flow Rate 3.3 L/min, T= 815°C

Table 6. Mass Transfer Coefficients at Different CO₂, Flow Rate 3.3 L/min, T= 815°C

CO ₂	N _{C,0} [moles]	CO _{2,bulk} [mole/m ³]	Slopes of plots [s ⁻¹]	Re	Sc	Experimental k _g [m/s]	k _{g,0} from Eqns 12 – 14 [m/s]
10 %	2.14	0.868	3.12 x 10 ⁻⁵	297	0.64	8.35x10 ⁻³	9.87x10 ⁻²
45 %	1.95	3.698	1.15 x 10 ⁻⁴	290	0.65	7.25x10 ⁻³	9.79x10 ⁻²
89 %	2.12	6.976	1.55 x 10 ⁻⁴	312	0.65	6.33x10 ⁻³	9.70x10 ⁻²

The Effect of Bed Temperature

The effect of bed temperature on the carbon consumption rate under an impinging jet of approximately 85% CO₂ concentration is presented in Figure 8 (exps 3, 8 & 9). Increasing the bed temperature increases the rate of organic carbon consumption. Each experiment experiences an initial plateau in which external mass transfer resistance is controlling the carbon consumption. In Figure 9 the carbon conversion is plotted for the three experiments. In the 675°C bed experiment the organic carbon consumption continues up to higher carbon conversions, suggesting that the gasification rate is more uniformly over the entire char bed surface. Table 7 summarizes the experimentally determined k_g values for the three temperatures. It shows that the coefficient of external mass transfer, k_g approximately doubles with each increase in temperature of about 70°C. This relatively small increase is further confirmation that the gasification rate is controlled by external mass transfer rather than by chemical kinetics. Again the experimentally determined value of k_g at 815°C is approximately one order of magnitude lower than the stagnation value determined by equations (12) – (14). However at the lower temperatures the stagnation mass transfer coefficient is virtually unchanged, as expected based on equations (12) – (14). This suggests that at the lower temperatures of 750°C but in particular at 675°C the gasification rate may also somewhat be affected by chemical kinetics.

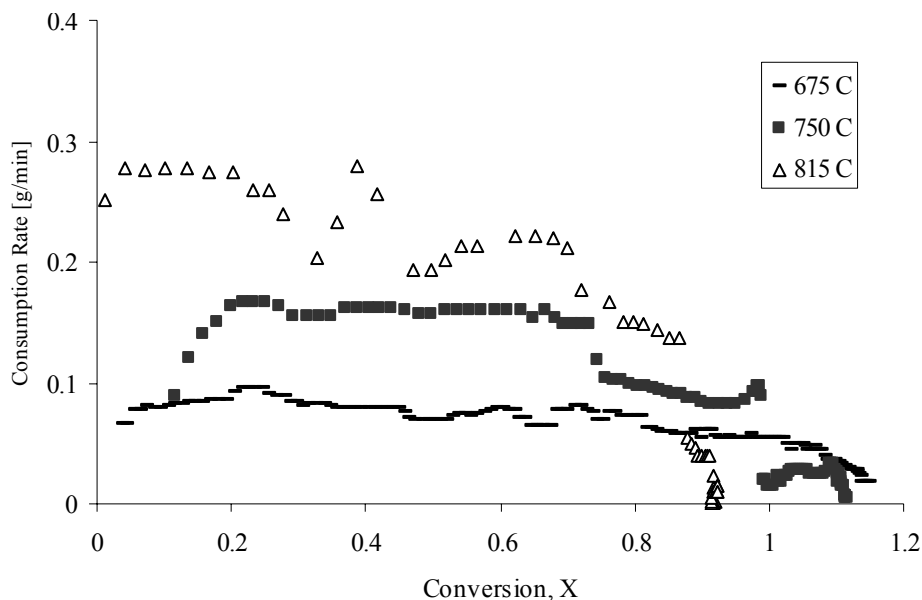


Figure 8. Organic Carbon Consumption Rates under Impinging Jets of 85% CO₂ Concentration at Varying Bed Temperatures, Flow Rate 3.3 L/min

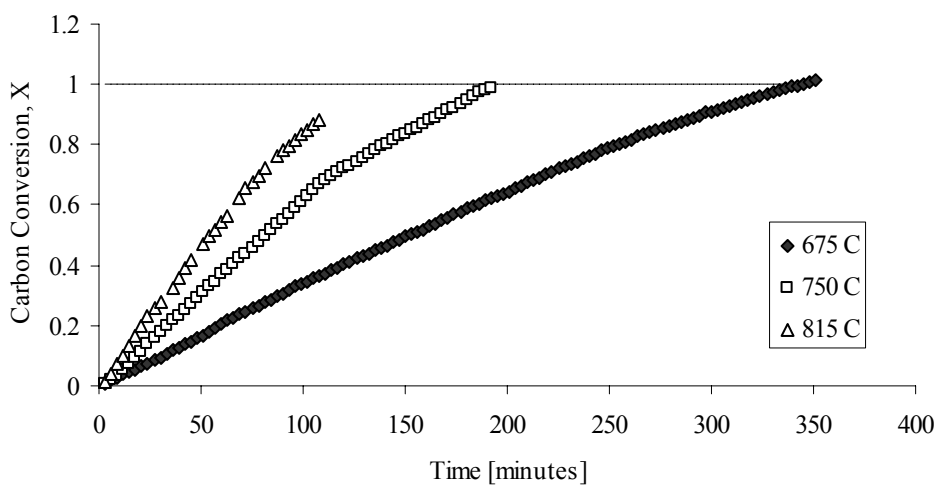


Figure 9. Organic Carbon Conversion under Impinging Jets of 85% CO₂ Concentration at Varying Bed Temperatures, Flow Rate 3.3 L/min

Table 7. Mass Transfer Coefficients at Different Temperatures

Temp [°C]	N _{C,0} [moles]	CO _{2,bulk} [mole/m ³]	Slopes of plots [s ⁻¹]	Re	Sc	Experimental k _g [m/s]	k _{g,0} from Eqns 12 – 14 [m/s]
675	2.06	10.180	5.47 x 10 ⁻⁵	276	0.75	1.63x10 ⁻³	7.87x10 ⁻²
750	1.97	7.323	1.05 x 10 ⁻⁴	248	0.69	3.79x10 ⁻³	7.76x10 ⁻²
815	2.12	6.976	1.55 x 10 ⁻⁴	312	0.65	6.33x10 ⁻³	9.70x10 ⁻²

The Effect of Bed Thickness

The effect of bed thickness under an impinging jet of approximately 85% CO₂ concentration on the carbon gasification rate is presented in Figure 10 (exps 3, 4 & 5). It can be seen that increasing the bed thickness decreases the rate of organic carbon consumption. A relatively constant rate during the initial gasification period suggests that external mass transfer resistance is the controlling mechanism of consumption. The external mass transfer coefficients are determined from the X-t plot, and the results are summarized in Table 8. The data clearly shows that the mass transfer coefficient decreases with increasing bed thickness. This is unexpected because theoretically the external mass transfer is not affected by the thickness of the char bed. Confirmation of this is seen by comparing the stagnation mass transfer coefficients calculated using equations (12) – (14) in Table 8. A possible explanation for the larger average mass transfer coefficient for the thinner beds could be that there is some gas penetration of the impinging jet into the char bed. The average k_g value was again approximately one order of magnitude lower than the stagnation value calculated using equations (12) – (14).

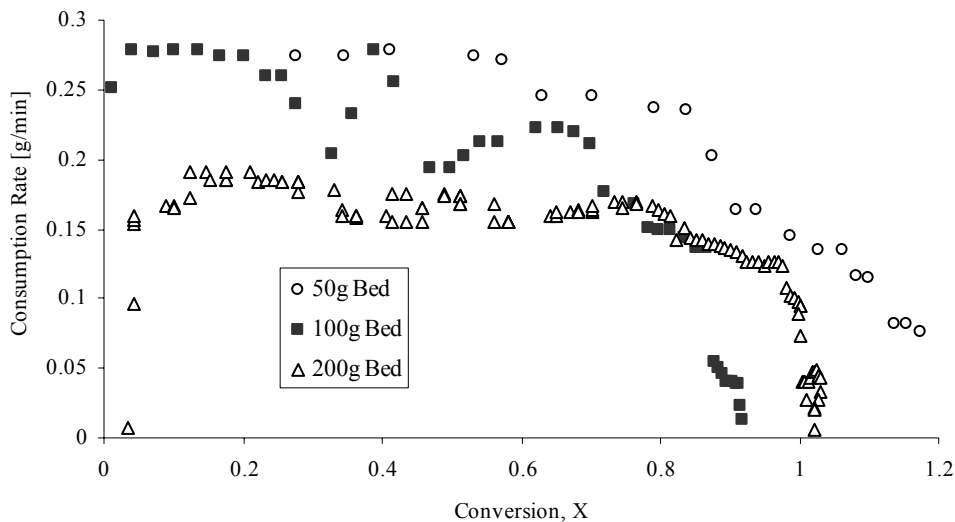


Figure 10. Organic Carbon Consumption Rates under Impinging Jets of 85% CO₂ Concentration at Varying Bed Mass, Flow rate 3.3 L/min, T= 815°C

Table 8. Mass Transfer Coefficients at Varying Bed Mass

Bed Mass [grams]	N _{C,0} [moles]	CO _{2,bulk} [mole/m ³]	Slopes of plots [s ⁻¹]	Re	Sc	Experimental k _g [m/s]	k _{g,0} from Eqns 12 – 14 [m/s]
50	1.01	5.945	3.83 x 10 ⁻⁴	300	0.67	7.92x10 ⁻³	1.01x10 ⁻¹
100	2.12	6.976	1.55 x 10 ⁻⁴	312	0.65	6.33x10 ⁻³	9.70x10 ⁻²
200	3.94	6.828	6.15 x 10 ⁻⁵	283	0.67	4.71x10 ⁻³	9.71x10 ⁻²

The Effect of Jet Velocity

In Figure 11 the data focusing on the effect of impinging jet velocity are presented (exps 3, 10 & 11). Increasing jet velocity increases the rate of organic carbon consumption. The carbon

consumption rate at the lowest impingement velocity of 1.0 L/min shows a significant variability. Furthermore, the gasification rate remained high until complete conversion. The 1.0 L/min experiment was conducted on a bed of 50 gram mass (10 mm thick) while the two higher flow rate experiments were performed with a 100 gram bed. Table 9 summarizes the mass transfer coefficients. The average mass transfer coefficient, k_g steadily increases with jet impingement, at almost the same rate as the stagnation point mass transfer coefficient calculated using equations (12) – (14). This is further confirmation that the gasification of carbon in the present set-up is controlled by external mass transfer.

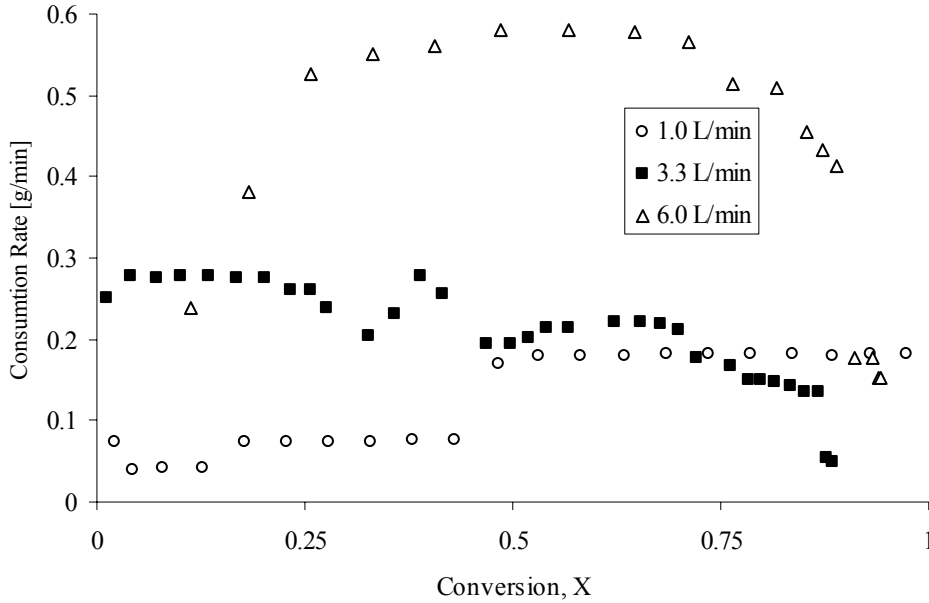


Figure 11. Organic Carbon Consumption Rates under Impinging Jets of 85% CO₂ Concentration at Varying Jet Velocities, Bed Temperature 815°C

Table 9. Mass Transfer Coefficients at Different Jet Velocities

Jet Velocity [L/min]	Bed Thickness [mm]	N _{C,0} [moles]	CO _{2,bulk} [mole/m ³]	Slopes of plots [s ⁻¹] x 10 ⁻⁴	Re	Sc	Experimental k _g [m/s]	k _{g,0} from Eqns 12 – 14 [m/s]
1.0	10	0.89	4.688	2.80	84	0.67	5.31x10 ⁻³	3.90x10 ⁻²
3.3	19	2.12	6.976	1.55	312	0.65	6.33x10 ⁻³	9.70x10 ⁻²
6.0	19	2.04	7.777	4.18	514	0.67	1.57x10 ⁻²	1.52x10 ⁻¹

Validating the Mass Transfer Limitation

The observed gasification rate can be described as (Levenspiel, 1996):

$$R_{CO_2, observed} = k_{CO_2} * C_{CO_2, bulk} * \epsilon_g * V_{bed} \quad (15)$$

where k_{CO_2} is defined by the Li and van Heiningen kinetics (1990) as:

$$k_{CO_2} = (Na/C) * C_{carbon,char} * 6.4e10 * \exp^{-30084/T} * (p_{CO_2} / (p_{CO_2} + 3.4 * p_{CO})) \quad (16)$$

and ϵ_g is the so called effectiveness factor

Combining equations (11), (15) and (16) one obtains an expression for ϵ_g :

$$\epsilon_g = \frac{k_g * \frac{P}{RT} * \ln\left(1 + \frac{RT}{P} * C_{CO_2,bulk}\right)}{k_{CO_2} * L * C_{CO_2,bulk}} \quad (17)$$

where L is the bed thickness ($=V_{bed}/S_A$)

The calculated values of ϵ_g are shown in Table 10 together with the experimentally determined values of k_g and $C_{CO_2,bulk}$. It shows that for all experiments ϵ_g is significantly smaller than 1.0, confirming that gasification is limited by external mass transfer and not by chemical kinetics.

Table 10 Validation of Mass Transfer Limitations

Exp	Gasification Gas	Bed Temp [°C]	Flow [L/min]	k_g , SCM [m/s]	$p_{CO_2,bulk}$ [atm]	k_{CO_2} [s ⁻¹]	$\epsilon_g \times 10^{-2}$
1	N ₂ , 10% CO ₂	815	3.3	8.35×10^{-3}	0.045	13.29	3.71
2	N ₂ , 44% CO ₂	815	3.3	7.25×10^{-3}	0.164	13.57	2.69
3	N ₂ , 89% CO ₂	815	3.5	6.33×10^{-3}	0.202	19.08	2.50
4	N ₂ , 83% CO ₂	815	2.9	7.92×10^{-3}	0.253	7.54	0.44
5	N ₂ , 84% CO ₂	815	2.9	4.71×10^{-3}	0.207	34.61	0.55
6	N ₂ , 15% CO ₂	815	4.5	1.10×10^{-2}	0.066	12.02	5.25
7	He, 18% CO ₂	815	4.1	1.23×10^{-2}	0.070	14.84	4.80
8	N ₂ , 85% CO ₂	675	2.9	1.63×10^{-3}	0.090	0.39	17.94
9	N ₂ , 88% CO ₂	750	2.8	3.79×10^{-3}	0.234	15.67	1.10
10	N ₂ , 85% CO ₂	815	1.0	5.31×10^{-3}	0.550	3.08	11.21
11	N ₂ , 85% CO ₂	815	6.0	1.57×10^{-2}	0.129	23.59	2.69

Bed Pictures

Figure 12 shows pictures of 3 char bed residues. In general the gasification experiments were performed until complete conversion of organic carbon was obtained based on the measured CO concentration in the off-gas. These char residues were generally solid, non porous discs with a pinkish-gray hue. The residue was sintered and normally receded 2mm from the aluminum oxide vessel walls. The bed volume decreased to about 33% of the original volume, while only losing 25% if the original mass (mostly organic carbon). In most cases there were no signs of remaining organic carbon, discrete black particles. When black organic carbon particles did appear it was near the outer bed edge.

		
<p>A) Represents a CO₂ gasification experiment performed at 815°C, under a 10% CO₂ jet. This experiment was not gasified completely. Un-reacted organic carbon seems to float on top of inorganic smelt.</p>	<p>B) Represents the residue of exp (8), CO₂ gasification at 675°C. This bed was unique in that the inorganic smelt contained discernable pores. Otherwise all gasification experiments yielded non-porous melt structures</p>	<p>C) Represents the side view of the residue smelt formed by exp (7), CO₂ gasification in Helium at 815°C. The black areas unique to the side of this smelt formation are organic carbon and illustrate the possibilities for non-uniform concentrations of organic carbon in the final bed.</p>

Figure 12 Bed Pictures after Gasification

Numerical Model

A numerical model of our impinging jet reactor is being developed using the COMSOL Multiphysics program. The governing equations of the model include the equation of continuity, the equation of motion, and the Maxwell-Stefan diffusion and convection mass balance. The gas is considered to be a mixture of three-components: CO₂, CO and N₂. At the interface between the gas and the bed, the concentration of CO₂ is considered to be zero and the molar flux of CO is twice that of CO₂ (based on stoichiometry) but in opposite direction. For the normal component of the gas velocity at the gas-bed interface, we considered two cases. In Case 1, it is assumed to be zero. In Case 2, it is determined from the fluxes of the components. Here we show the results of Case 1; Case 2 is under development. Figure 13 presents the radial position profile of CO₂ mass transfer coefficients determined by the model at the bed surface for impinging jets containing 15% CO₂. The Reynolds Numbers are calculated for the inlet tube. Average k_g values were determined from surface integrals over the disk to compare with the experimentally determined k_g . Table 11 presents average k_g values determined for impinging jets of 15 % CO₂. If we compare the model calculated value to that of experiment 6 we see that the model calculated k_g value of 2.64×10^{-2} m/s is higher but at the same order of magnitude as the experimentally determined value of 1.10×10^{-2} m/s. This suggests that the net gas outflow from the char bed due to carbon gasification may lead to a reduction of almost 60% in the mass transfer coefficient.

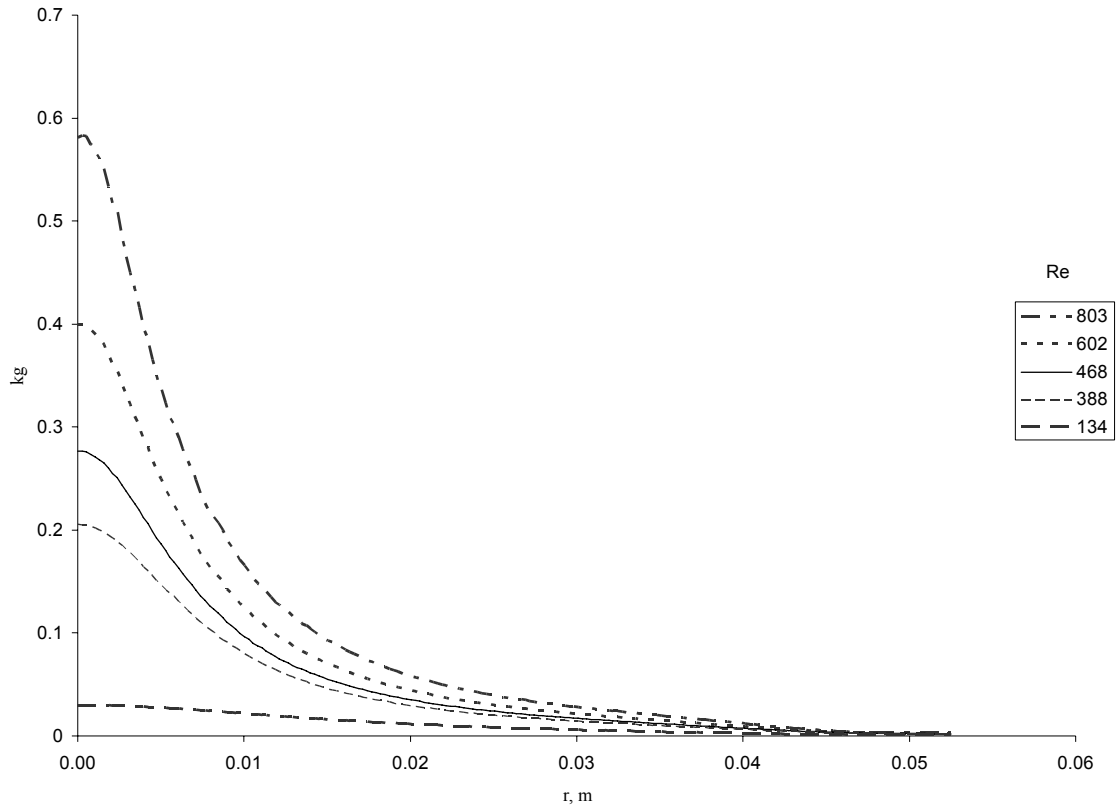


Figure 13 CO₂ mass transfer coefficients at the char bed surface of impinging jets (15% CO₂) of varying flow rates (expressed in Reynolds Numbers) at radial positions of the bed. The bed has a radius of 0.0525 m and the stagnation point of the impinging jets is at $r = 0$.

Table 11. Average k_g values determined by the model for 15% CO₂ feed

Jet Flow rate [L/min]	Re	Average k_g [m/s]
6.0	803	3.50×10^{-2}
4.5	602	2.64×10^{-2}
3.5	468	2.06×10^{-2}
2.9	388	1.72×10^{-2}
1.0	134	5.96×10^{-3}

Conclusions

A pilot char bed reactor was constructed to study the gasification of black liquor char by CO₂. Organic carbon was gasified by CO₂ supplied as a jet impinging on the top surface of the char bed. The experimentally determined gasification rates are very low, suggesting that the process is controlled by mass transfer resistances. The gasification process was described by the shrinking

core model with external diffusion control. After the initial constant rate period, the carbon gasification rate decreases most likely due to the non-uniform carbon gasification leading to complete carbon burnout in the impingement region before that in the regions away from the stagnation region. A numerical model which does not account for out flow from the impingement surface predicts k_g values that are comparable with those obtained from the experimental data. This suggests that the net gas outflow from the char bed due to carbon gasification may lead to a large further reduction in the mass transfer coefficient.

References

- Borg, A., Teder A. & B. Warnqvist*, "Inside a kraft recovery furnace-studies on the origins of sulfur and sodium emission", Tappi Journal, 1974, 57(1):126-129.
- Brown, C., T. Grace, S. Lien, and D. Clay*, "Char-bed burning rates- experimental results", Tappi Journal, October, 1989, pp. 175-181.
- Connolly, T.S. & van Heiningen A.R.P.*, "Measurement of Gas Composition inside a Recovery Boiler Char Bed", Int. Chemical Recovery Conf., Proc., Tappi Press (2004).
- Da Silva, Luiz C.C.*, "Thermodynamic Fundamentals of Reduction of Iron Oxides", ABM (assoc. brasil. metais), 1960: 16(60):617-640.
- Grace, T. M.*, "A Review of Char Bed Combustion", International Chemical Recovery Conference Proceedings (Oral Presentations), June 11-14, 2001: 215-220
- Grace, T.M. & W.J. Frederick*, "Char Bed Processes", Chapter 6 in Kraft Recovery Boilers, Adams, T.N. Ed., Atlanta, GA: Tappi Press(1997).
- Kochesfahani, S.H., Tran, H., Jones, A., Grace, T., Lien, S. & Schmidl, W.*, "An Experimental Study of Black Liquor Char Bed Burning", Int. Chemical Recovery Conf., Proc., Tappi Press 1998:209-220.
- Lee, S.R. and K.M. Nichols*, "CO₂ Gasification of Kraft Black Liquor Char in a Fixed-Bed Reactor", Journal of Pulp and Paper Science, Vol. 23, No. 3, March 1997, pp. J132-J137.
- Levenspiel, O.*, The Chemical Reactor Omnibook, 5th ed., 1996.
- Li, J. & van Heiningen A.R.P.*, "Kinetics of CO₂ Gasification of Fast Pyrolysis Black Liquor Char", Ind. Eng. Chem. Res., 1990, 29(9):1776-1785.
- Merriam, R.L. & D.L. Richardson*, Study of Cooling and Smelt Solidification in Black Liquor Recovery Boilers. Cambridge, Ma: Arthur D. Little, Inc; 1977 Feb; ISBN: hrl.
- Merriam, R.L. & D.L. Richardson*, Study of Cooling and Smelt Solidification in Black Liquor Recovery Boilers Phase II. Cambridge, Ma: Arthur D. Little, Inc; 1978 Dec; ISBN: hrl.

Popiel, C.O., van der Meer, T.H., & C.J. Hoogendoorn, “Convective Heat Transfer on a Plate in an Impinging Round Hot Gas Jet of Low Reynolds Number”, *International Journal of Heat & Mass Transfer*, 1980, 23:1055-1068.

Saad, N.R., Douglas, W.J.M . , & A.S. Mujumdar, “Prediction of Heat Transfer under an Axisymmetric Laminar Impinging Jet”, *Fundamentals of Industrial Chemical Engineering*, 1977, 16(1):148-154.

Sutinen, J., Karvinen, R. & W.J. Frederick, “A Chemical Reaction Engineering and Transport Model of Kraft Char Bed Burning”, *Ind. Eng. Chem. Res.*, 2002, 41:1477-1483.